JOURNAL OF APPLIED METEOROLOGY AND CLIMATOLOGY

Confronting intensity scaling to quantile mapping for the real time correction of satellite-based rainfall estimates: test over French Guiana

DAVID BROCHART*

UR HBAN, Irstea, Antony, France

VAZKEN ANDRÉASSIAN

UR HBAN, Irstea, Antony, France

CHARLES PERRIN

UR HBAN, Irstea, Antony, France

MAXIME MONFORT

DEAL Guyane, Cayenne, French Guiana

ABSTRACT

Satellite precipitation products are known to be plagued by large biases, which limit their use for operational applications. This paper presents a robust approach to adjust the satellite-based rainfall estimates using an intensity-dependent error correction curve (intensity scaling), determined by taking the mean of historic ground measurements given the satellite estimates (conditional mean). We apply the procedure to seven satellite precipitation products over French Guiana and present a double validation, first at the raingage scale, and then at the catchment scale. Over the six catchments used here, the rainfall-runoff simulations are considerably improved when the correction is applied, outperforming the well-established quantile mapping technique.

1. Introduction

a. Context

Satellite-based rainfall estimates can be extremely useful on large international catchments: satellites can simultaneously see across international borders and provide a near real time representation of precipitations, with high spatial and temporal resolution. The main reason that prevents them from being used for operational applications is their rather poor accuracy, compared to ground-based measurements (**??**). In this paper, we attempt to overcome this limitation and propose a method for correcting satellite-based estimates using the available sparse raingage network. For the sake of generalizability, we tested seven satellite products (TRMM-3B42RT, TRMM-3B42, PERSIANN, PERSIANN-GCCS, PERSIANN-CDR, CMORPH-RAW, and CMORPH-CRT) over a large territory, French Guiana. To demonstrate the hydrological potential of this approach, we used the corrected rainfall as an input to a hydrological model, thus allowing a streamflow-based validation of rainfall correction.

*Corresponding author address: David Brochart, UR HBAN, Irstea, 1 rue Pierre-Gilles de Gennes, Antony, France.
E-mail: david.brochart@gmail.com

b. Satellite rainfall measurements

We will not provide here an exhaustive review of satellite-based rainfall measurement, which can be found in recent papers (**??**). For this paper, we will only mention that satellite-based rainfall is estimated from two kinds of measurement.

1) INFRARED MEASUREMENTS (IR)

Thermal-infrared imaging measures the brightness temperature of the clouds' top layer. High-level clouds are colder than low-level clouds, and the colder a cloud, the more likely it is to precipitate. This is a rather poor correlation, but the advantage of IR measurements is that they are provided by geostationary satellites, which always "see" the same Earth disk, which is scanned approximately every 30 min. IR measurements also have a good spatial resolution (about 4 km at the equator).

2) MICROWAVE MEASUREMENTS (MW)

Microwave imagers are embedded in polar-orbiting satellites. Passive microwave sensors detect the naturally emitted microwave energy of the Earth through the clouds,

part of which is attenuated by precipitations. The correlation with rainfall is much stronger than for IR measurements, but the temporal resolution is significantly lower (the Earth is scanned less than once per day). The TRMM satellite also embeds a precipitation radar (active microwave).

In combining both measurement types through various techniques, satellite rainfall products take advantage of the quality of MW data and the good sampling frequency (in space and time) of IR data.

c. Previous studies

The advantage of using satellite-based rainfall estimates for hydrological forecasting is obvious. Satellites offer global coverage (usually 50°S - 50°N), a typical temporal resolution of 3 h (up to 30 min), and a typical spatial resolution of 0.25°(up to 0.04°), with virtually no missing data. Their estimates are freely available on the Internet, in near real time (for some of the products). They could advantageously complement ground raingage networks or be used where no raingage network is available, if only they offered more accurate estimates.

It has been reported that satellite rainfall products that are primarily MW-based, namely TRMM and CMORPH (see section **??**), are more accurate than products that are primarily IR-based, namely PERSIANN (**?**), because of the more direct relationship between MW measurements and rainfall. However, as pointed out by **?**, there is no "best product": they all have their strengths and weaknesses, and their performance differences are often only marginal. Therefore, it should be remembered that satellite-based rainfall estimates remain relatively uncertain, i.e., not only do they exhibit systematic biases, but they are also altered by random errors.

? mentioned that the accuracy of satellite-based rainfall estimates increases as the space scale and the time scale expand, especially for products that are bias-corrected. This is because random errors tend to cancel out when averaging in space or time. Bias-correction typically uses ground-based observations over a calendar month (as for TRMM-3B42), and so bias-corrected satellite estimates are usually available after a 1-month delay. However, for near real time products, which are not bias-corrected, there is still a need to reduce bias without losing the real time function or decreasing the spatial and temporal resolution.

Often, some kind of ground precipitation data is or has been available, but for several reasons it cannot be used in real time. We think that there is room for a satellite-based precipitation estimate bias reduction model, simple and robust enough to efficiently take advantage of the ground information provided even by a very sparse raingage network for its calibration, with no need for real time ground measurements. In the literature, this objective has been addressed using a quantile mapping technique (**?**). For this reason, we will use quantile mapping as a benchmark to evaluate the efficiency of the intensity scaling method proposed in this article.

d. Scope of the paper

This paper is organized in three main parts. We first introduce the methods we propose to test for the correction of satellite-based rainfall estimates (section **??**), followed by the material used to apply and validate the methods: the satellite rainfall products, the ground raingage network and the hydrometric network (to be used for catchment-scale validation) (section **??**). The application of the method to French Guiana is then presented (section **??**), first globally on the entire country, and then gradually refining its dependence with seasons and regions. Validation results are given successively using a point comparison with the raingage measurements and a basin-scale comparison with streamflow measurements. Each time, the quantile mapping technique is used as a benchmark.

2. Methods

a. Reference adjustment method: quantile mapping

Quantile mapping is a technique that attemps to find a transformation of a signal (in this context, the satellite-based rainfall estimates), such that its new distribution equals the distribution of another signal (here, the raingage-based ground truth). This technique was used for instance by **?** for the adjustment of satellite precipitation data. However, as pointed out by **?**, when applying quantile mapping to e.g. TRMM-3B42RT rainfall estimates, part of the rainfall range is censored, as shown in Figure **??**. This is because satellite-based rainfall estimates commonly suffer from an overestimation of the zero rain rate, a phenomenon that can be explained by the fact that the first step in IR image processing is to put a threshold on the brightness temperatures: if a pixel is warmer than the threshold value, it is considered as not precipitating. In a number of cases, this will not be true. The deficiency may also come from the relatively low temporal frequency of IR image acquisition, about every 30 min. This could be insufficient for convective rainfall, the most common type of rainfall in the tropics. In particular, for unicellular storms ("popcorn" convection), the clouds' life-cycle, from their formation to their precipitation, ranges from 30 to 50 min (**?**). It is likely that some of these storms are not captured by satellites.

It would be legitimate to apply quantile mapping if the transformed distribution could span the complete range of the rainfall ground truth, but because the lower rainfall range is truncated, fitting the rest of the distribution will inevitably result in an overestimation of low rainfall intensities, which will lead to a positive bias. To overcome

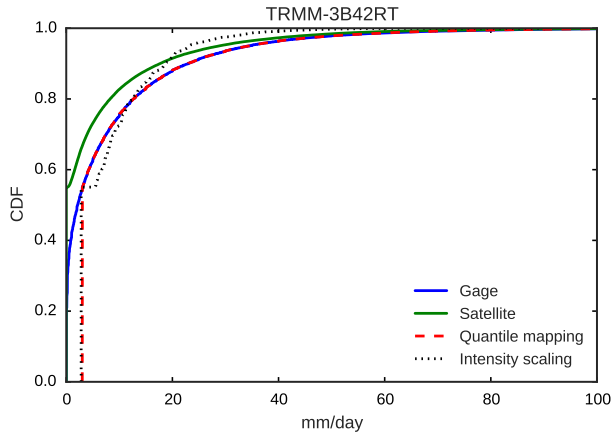

FIG. 1. Cumulative distribution function of the raingage measurements (in blue) and the TRMM-3B42RT rainfall estimates in pixels that contain a raingage (green line, original; red dashed line, after quantile mapping correction, and dotted black line, after intensity scaling correction).

this limitation of the quantile mapping technique, we propose the intensity scaling technique, which is based on the estimation of the conditional mean.

b. Adjustment based on intensity scaling

The intensity scaling correction proposed here makes the assumption that the satellite-based rainfall estimates are mainly altered by a signal distortion, i.e., their bias depends on their intensity. When representing the satellite estimates (the noisy signal) and the corresponding ground truth on a scatter plot, the points are not aligned on the 1:1 line, as they would be if there were no error.

Consider the example illustrated in Figure **??**. The left graph represents the scatter plot of a noisy satellite precipitation estimate (P_{Noise}) as a function of the ground truth (P_{Truth}). For the purpose of clarity, the distribution of P_{Noise} was chosen to be uniform between 0 and 100 mm/day, and the noise affecting P_{Truth} was chosen to be purely additive, consisting of a random centered uniform noise and a systematic noise that depends linearly on P_{Truth} (negative for $P_{Truth} < 50$ mm/day, positive for $P_{Truth} > 50$ mm/day). Given a particular range of satellite rainfall intensities (in red for $40 < P_{Noise} < 60$ mm/day), it is possible to select all the possible rainfall intensities that were measured by the raingages (P_{Truth}). By reducing the P_{Noise} window and taking the average of the corresponding P_{Truth} values, we obtain the mean value of P_{Truth} when we observed P_{Noise}. Because the random noise tends to cancel out when averaging, this method is an effective means to remove bias. This process can be repeated for all possible P_{Noise} values by applying a rolling mean along its axis. What is left, as shown in the right plot in Figure **??**, is a simple yet robust correction curve, which gives the corrected value corresponding to an observed P_{Noise} value.

It can be noted from Figure **??** that there is a singularity for $P_{Noise} = 0$: the corrected value for this point is not continuous with the correction curve for $P_{Noise} > 0$. This is because the precipitation intensities cannot take negative values. At this point, the precipitation estimate errors overlap, resulting in a complex error structure. However, it can still be treated by simply taking the mean of P_{Truth} when $P_{Noise} = 0$. Thus, in the correction method, two cases will be considered: when $P_{Noise} = 0$, the corrected value will be taken as the mean over the corresponding P_{Truth} values, and when $P_{Noise} > 0$, a rolling mean of the P_{Truth} values along the P_{Noise} axis will be used.

This method is intensity-dependent: it does not apply the same transformation to all rainfall ranges (e.g., through a scaling factor). It is an implementation of the conditional expectation, here the mean value of the rainfall ground truth given the satellite-based rainfall estimates. Quantile mapping is also an intensity-dependent transformation, but because it aims at matching one signal distribution to another signal distribution (which is impossible in this context because of the threshold effect of zero values), it does not explicitly attemp to correct the signal distortion. The method we propose takes into account the loss of information in the satellite-based rainfall estimates for low rainfall estimates, which is essential from a catchment water balance point of view. Figure **??** shows that the distribution of satellite-based rainfall estimates corrected with the intensity scaling method does not match the distribution of the rainfall ground truth. We believe this is not a problem since it cannot be done anyway. Rather than focusing on this impossible task, our method attempts to approximate the true signal the best it can, while respecting the catchment water balance.

This method shows similarities with the method proposed by **?**. However, our approach differs in a way we believe is quite important in practice. Instead of applying Bayes' theorem in order to determine the conditional probability of the rainfall ground truth given the satellite-based rainfall estimates, and then the most probable value of the rainfall ground truth (maximum likelihood), we directly compute the mean value of the rainfall ground truth given the satellite-based rainfall estimates (conditional mean). Aside from being much simpler to implement (this is just a rolling mean), the conditional mean does not suffer from the problems encountered by **?** when faced with the difficulty to determine the most probable value of the conditional probability, making their method potentially less robust. Furthermore, the maximum likelihood estimator does not guarantee that the ground truth and the corrected satellite-based rainfall estimates average to the same value: in other words, it is not a good means of bias reduction. On the contrary, the conditional mean

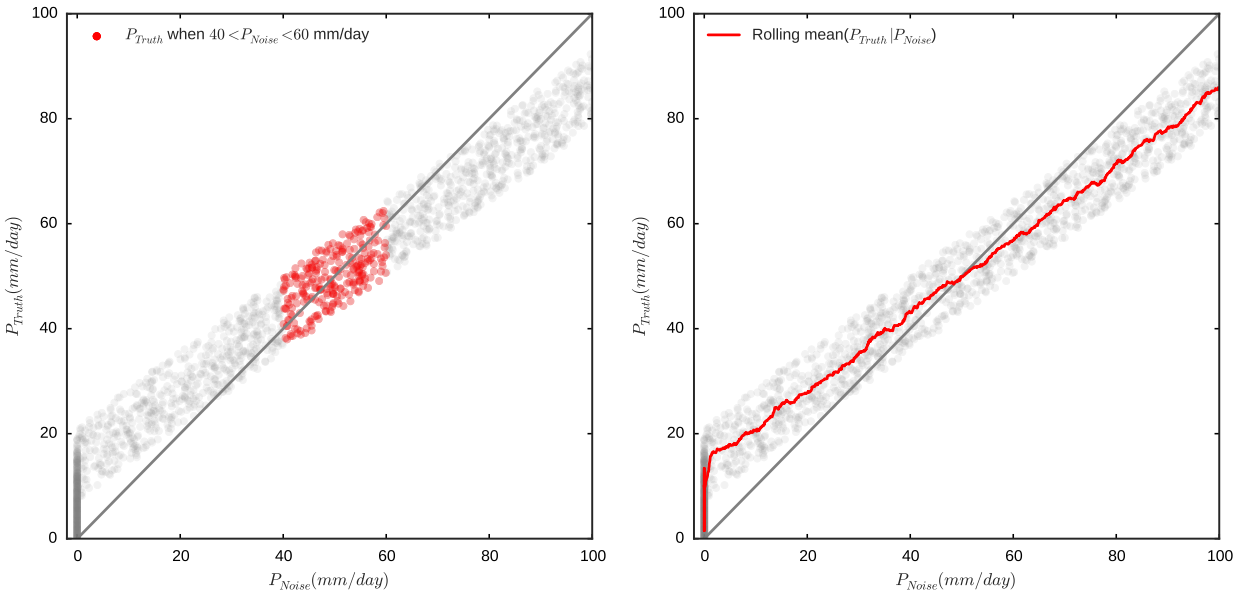

FIG. 2. Example of rainfall estimates affected by a simple additive random and systematic noise (P_{Noise}). Left: selection of the ground truth (P_{Truth}) corresponding to a given P_{Noise} range. Right: the rolling mean can filter out the random errors and identify the bias. The result is a correction curve.

estimator achieves this goal because it is designed to do so by construction.

c. *Evaluation approach*

Each raingage can be located within one pixel of the grid of satellite-based precipitation products. Depending on the resolution of the satellite estimates, there can be one or several raingages within a satellite pixel. When there are several raingages within a pixel, the daily mean of each rainfall time series will be assigned to the resulting *raingage pixel*.

Each raingage pixel will be used as a ground truth for the evaluation of the precipitation products, and satellite pixels will directly be compared to raingage pixels at the daily time step. The scale difference between the two pixel types should not be seen as an incompatibility. It is true that a satellite pixel can encompass an area as large as 800 km^2, which already represents an average over this area. Ideally, the raingage data should be processed to make them match the satellite scale using geostatistical methods, as is done for example by **?**. Here we chose to treat the raingage data as is. The scale discrepancy is seen as another source of uncertainty that contributes to the wide scatter between the two data sources.

Once the correction curve has been determined, the corrected satellite-based rainfall estimates are evaluated using a point comparison with the raingage measurements at a daily time step. The Pearson correlation coefficient, the mean ratio, and the standard deviation ratio between the satellite-based and the raingage-based rainfall estimates are given for original satellite estimates (i.e., before correction), satellite estimates after quantile mapping correction, and satellite estimates after intensity scaling correction.

An areal validation is done over six gauged catchments in French Guiana, using a hydrological model calibrated with observed streamflows and satellite-based rainfall estimates, before and after both corrections. Nash-Sutcliffe efficiency (**?**) is used to evaluate the model's performance. The capacity of the hydrological model to reproduce the observed streamflow from the corrected rainfall indirectly reflects the quality of the rainfall time series (**?**). This is true provided that the model structure can be applied to the catchment considered, and that the model does not compensate for the errors in the rainfall time series.

3. Material

a. *Satellite rainfall estimates*

Seven satellite precipitation products were tested in this study (see Table **??**). They are based on the three following families of products.

1) TRMM

Tropical Rainfall Measuring Mission (**?**) is a joint mission between the National Aeronautics and Space Administration (NASA) and the Japan Aerospace Exploration Agency (JAXA). It is both a satellite and a series of products that use this satellite (as well as other satellites). Among these products, TRMM-3B42RT is a near real

time rainfall estimate product with a spatial resolution of 0.25°(≈ 28 km at the equator) and temporal resolution of 3 h. It uses MW estimates when available and IR estimates otherwise. IR estimates are calibrated using MW estimates to ensure they are consistent with each other. A version called TRMM-3B42 uses raingage measurements over a calendar month for IR calibration and is thus not available in real time.

2) PERSIANN

Precipitation Estimation from Remotely Sensed Information using Artificial Neural Networks (**?**) was developed at the University of California, Irvine, and uses a neural network technique that learns from MW and ground measurements for IR calibration, but then only uses IR measurements to produce its estimates. Its resolution is 0.25°- 3 h. A version called PERSIANN-GCCS (Global Cloud Classification System) offers a higher resolution of 0.04°(4.5 km at the equator) - 1 h. PERSIANN-CDR (Climate Data Record) covers a 30-year period (from 1983). Its resolution is 0.25°- 1 day. Only PERSIANN-GCCS is available in near real time (PERSIANN is available with a 2-day delay).

3) CMORPH

The CPC MORPHing technique (**?**) was developed at NOAA's Climate Prediction Center. For this product, MW measurements are the primary source of rainfall estimates, and IR measurements are used to propagate these estimates using a morphing technique. There are two versions: V1.0-CRT, which is bias-corrected and uses daily raingages (and not real time), and V1.0-RAW, which is not bias-corrected (available with an 18-h delay). There is also a version called QMORPH, which is available within 3 h of real time. Their resolution is 0.07°(8 km) - 30 min. In this paper, only V1.0-RAW and V1.0-CRT were tested (no records are available for QMORPH).

b. Study area

Located between 2°N and 6°N (see Figure **??**), French Guiana has a tropical wet climate. The precipitation regimes are based on the seasonal movements of the Intertropical Convergence Zone (ITCZ). As such, the rainy season lasts from December to July, with a peak in May and a dryer month in March, and the dry season lasts from August to November.

According to the expertise of local meteorologists at Météo France, French Guiana can be divided into two main climatic regions: the coast and the inland areas. The coast is under the influence of wet oceanic air masses, and therefore receives a greater amount of rainfall than the inland. Annual rainfall amounts of 3000 mm or more are typical for the coast, while they are around 2500 mm in the inland. Within the wet coastal region, a very wet subregion can be identified. Located in northeastern French Guiana near Regina, it receives the highest annual amount of rainfall. A record of 5678 mm was measured in the year 2000 by the Camp Caiman raingage, north of Kaw Mountain. The particularity of the Regina region may result from several factors:

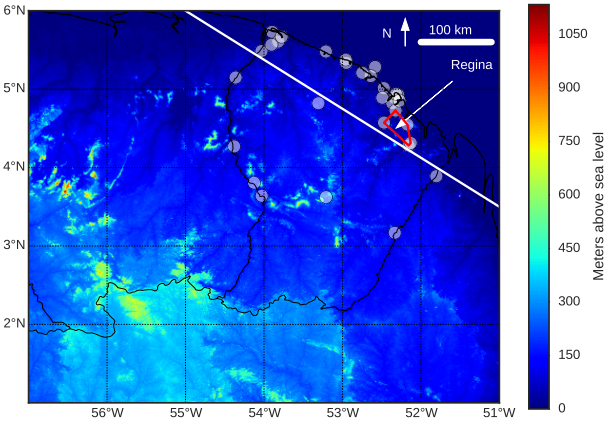

FIG. 3. French Guiana's elevation and the Regina region in the northeast (defined by the red polygon), where the highest annual amount of rainfall is observed. The white line delimits the inland and the coast areas. The white circles show the locations of the raingages.

1. During the rainy season, the ITCZ strikes the northeast of French Guiana first.

2. There is a likely influence of Kaw and Roura mountains despite their modest elevation (orographic effect).

3. The presence of the Kaw marshes increases the region's humidity, which is likely to generate further rainshowers.

c. Raingage network

The location of the 31 raingages used for the correction method calibration and for the point validation is shown in Figure **??**. Daily precipitation time series are available from 2000-01-01 to 2014-01-01. Time series are complete for 28 raingages: two time series are 99% complete and one is 93% complete. None of these raingages is available in real time.

d. Potential evapotranspiration

In his study of the actual evapotranspiration over the equatorial forest of French Guiana, **?** gives average monthly potential evapotranspiration values using the Penman equation. We used these values for the hydrological validation, downscaled to a daily time step, assuming that

TABLE 1. Characteristics of the seven tested satellite products. The given equivalences between degrees and kilometers are valid near the equator.

Product	TRMM 3B42RT	TRMM 3B42	PERSIANN	PERSIANN GCCS	PERSIANN CDR	CMORPH RAW	CMORPH CRT
Developer	NASA/JAXA	NASA/JAXA	UC Irvine	UC Irvine	UC Irvine	CPC NOAA	CPC NOAA
Resolution	0.25°≈ 28 km 3 h	0.25°≈ 28 km 3 h	0.25°≈ 28 km 3 h	0.04°≈ 4.5 km 1 h	0.25°≈ 28 km 1 day	0.07°≈ 8 km 30 min	0.07°≈ 8 km 30 min
Availability	From 2000-03	From 1998-01	From 2000-03	From 2003-01	From 1983-01	From 1998-01	From 1998-01
Real time	Yes	No	No	Yes	No	Yes	No

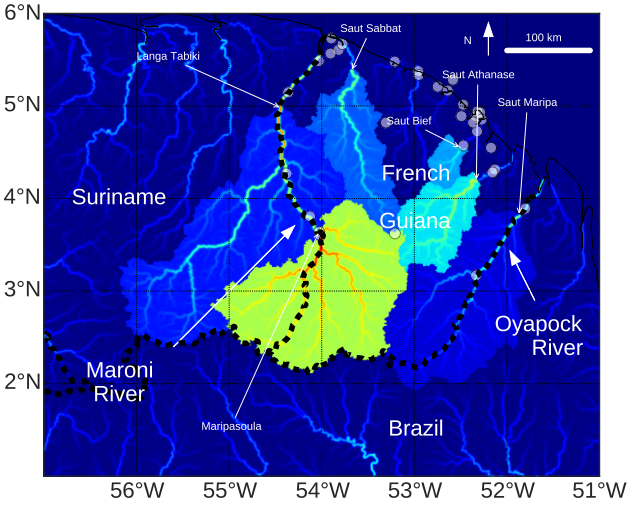

FIG. 4. French Guiana: administrative boundaries (dashed lines), the six gauging stations and their corresponding catchments (colored areas), and the 31 raingages (white circles).

they are constant over a calendar month and over all of French Guiana. This approximation has a limited impact on the performance of the hydrological model used here, as shown by **?**.

e. Streamflow

The six catchments used for the hydrological validation are shown in Figure **??**. Their characteristics are summarized in Table **??**. Because the catchments lie inland (where the raingage density is extremely low), streamflow adds a valuable complementary validation method to the point validation, which lacks references inland. Here the catchment can be seen as an imperfect raingage with at least one advantage: it covers its entire area.

f. Hydrological model

A hydrological model is used to transform rainfall (corrected and uncorrected) into streamflow. We used the GR4J model (**?**). It is a daily lumped rainfall-runoff model

TABLE 2. Characteristics of the six gauged catchments in French Guiana. NA stands for missing values in the daily streamflow time series and is given for the 2000-01-01 to 2012-02-12 period.

River	Hydro. station	Area (km^2)	% NA
Maroni	Langa Tabiki	60930	16
Lawa	Maripasoula	28285	26
Oyapock	Saut Maripa	25120	43
Mana	Saut Sabbat	10255	44
Approuague	Saut Athanase	7525	34
Comté	Saut Bief	1760	2

with four parameters to calibrate. Its inputs are daily evapotranspiration (PE) and rainfall (P) time series, and its output is a daily discharge time series (Q). The calibration is made using a Nelder-Mead simplex algorithm (**?**).

4. Results

a. Point-scale evaluation of rainfall adjustment

1) GLOBAL CORRECTION

Here we consider all the available raingage pixels together, and we wish to determine a global correction curve that will be applied to all of French Guiana, any time of the year. Figure **??** shows the probability distribution for the raingage-based rainfall estimates (P_{gage}) when the corresponding satellite-based rainfall estimates (P_{sat}) are zero (left plot), and the joint probability distribution for the raingage-based rainfall estimates and the corresponding satellite-based rainfall estimates when both are not zero (right plot), for TRMM-3B42RT. In the joint probability distribution plot, a logarithm scale was used for the daily precipitation values, which better fits their distribution. On top of this graph, we show in red the rolling mean of P_{gage} along the P_{sat} axis. This is the correction curve for non-zero P_{sat} values. Such a correction curve was previously reported in the literature (**?**), with the same characteristics (underestimation of small rainfall intensities, overestimation of large rainfall intensities). The corrected satellite value of the zero P_{sat} value is shown as a red dot (even though it cannot be represented on a logarithm scale). It corresponds to the mean of P_{gage} when $P_{sat} = 0$, and it is represented as a red vertical dashed line on the left plot.

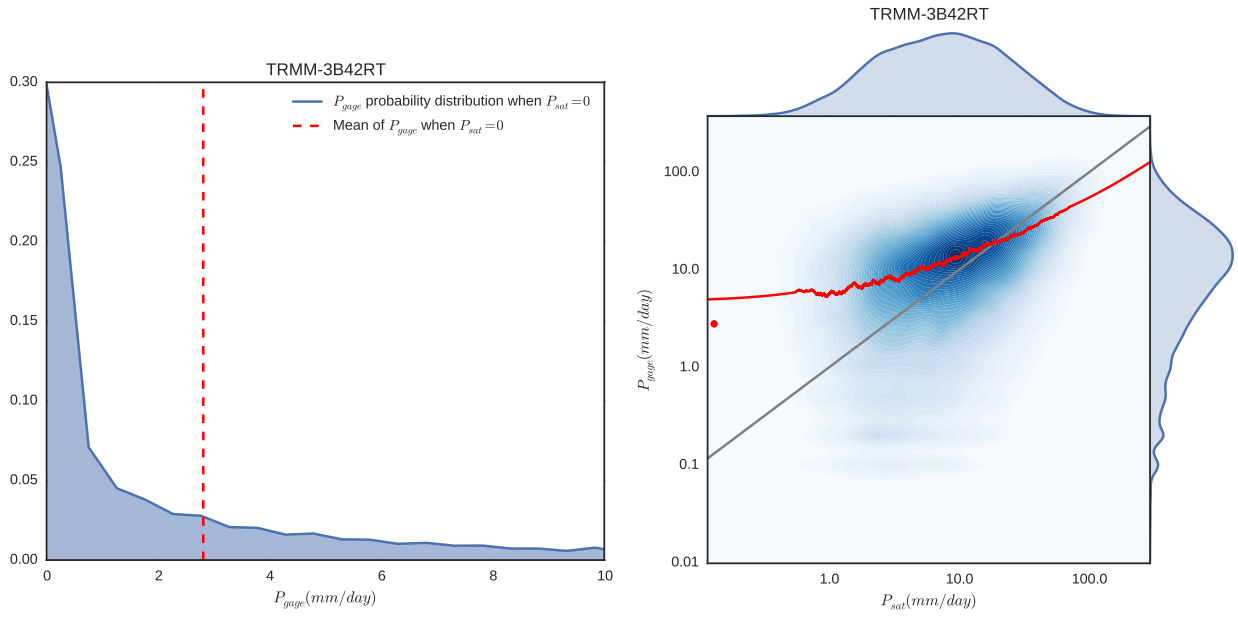

FIG. 5. TRMM-3B42RT global correction curve. Left: probability distribution of the raingage measurement values (P_{gage}) when the satellite pixel values are zero ($P_{sat} = 0$). The red vertical dashed line shows the mean. Right: joint probability distribution for the satellite pixel values (P_{sat}) and the raingage measurement values (P_{gage}). The red curve represents the correction curve for $P_{sat} > 0$, and the red dot the corrected satellite value for $P_{sat} = 0$.

The point evaluation of the global correction is shown in Figure **??** (left). The intensity scaling correction gives better performance than the quantile mapping correction in terms of the Pearson correlation coefficient but not in terms of the standard deviation ratio, for which the performance is even worse than without correction. This is a typical trade-off that is well known in noise reduction systems: noise can only be removed at the expense of the signal variability, resulting in signal smoothing. It should be remembered that the standard deviation of the raingage-based rainfall estimates is expected to be greater than for the satellite-based rainfall estimates, which are averaged over a pixel area. This is why the apparently good results in terms of standard deviation after quantile mapping correction should be interpreted with caution: the increase in standard deviation when the standard deviation of the original satellite-based rainfall estimates is lower than for the raingage-based rainfall estimates is likely to be artificial, because imputable to the amplification of the noise variability. On the other hand, the mean perfectly equals the mean of the raingage-based rainfall estimates after intensity scaling correction, because it was designed to do so by construction. For the quantile mapping correction, there is an overestimation of the mean (positive bias), as expected (see section **??**).

2) MONTHLY DEPENDENT CORRECTION

Because the precipitation regimes follow a seasonal cycle, it is reasonable to assume that the errors of the satellite precipitation estimates follow the same pattern. It is indeed a common practice to analyze the satellite precipitation estimate errors as a function of the season (**?**). Figure **??** shows the correction curve for TRMM-3B42RT for the months of May and November, the wettest and the driest months, respectively. There is clearly a monthly dependence.

3) REGIONALLY DEPENDENT CORRECTION

As mentioned in section **??**, there are three climatically different regions in French Guiana: the coast, the inland, and the coastal Regina sub-region. This spatial pattern is reflected in the spatial errors of the satellite precipitation estimates, as shown in Figure **??**.

To better take into account the spatial variability of the satellite-based error estimates, we compute a correction curve for each region. Figure **??** shows the delineation of the regions: the inland and the coast are delimited by the white line, and the Regina region is defined by the red polygon. Figure **??** shows the correction curve for TRMM-3B42RT for the three regions. Here again, there is clearly a regional dependence.

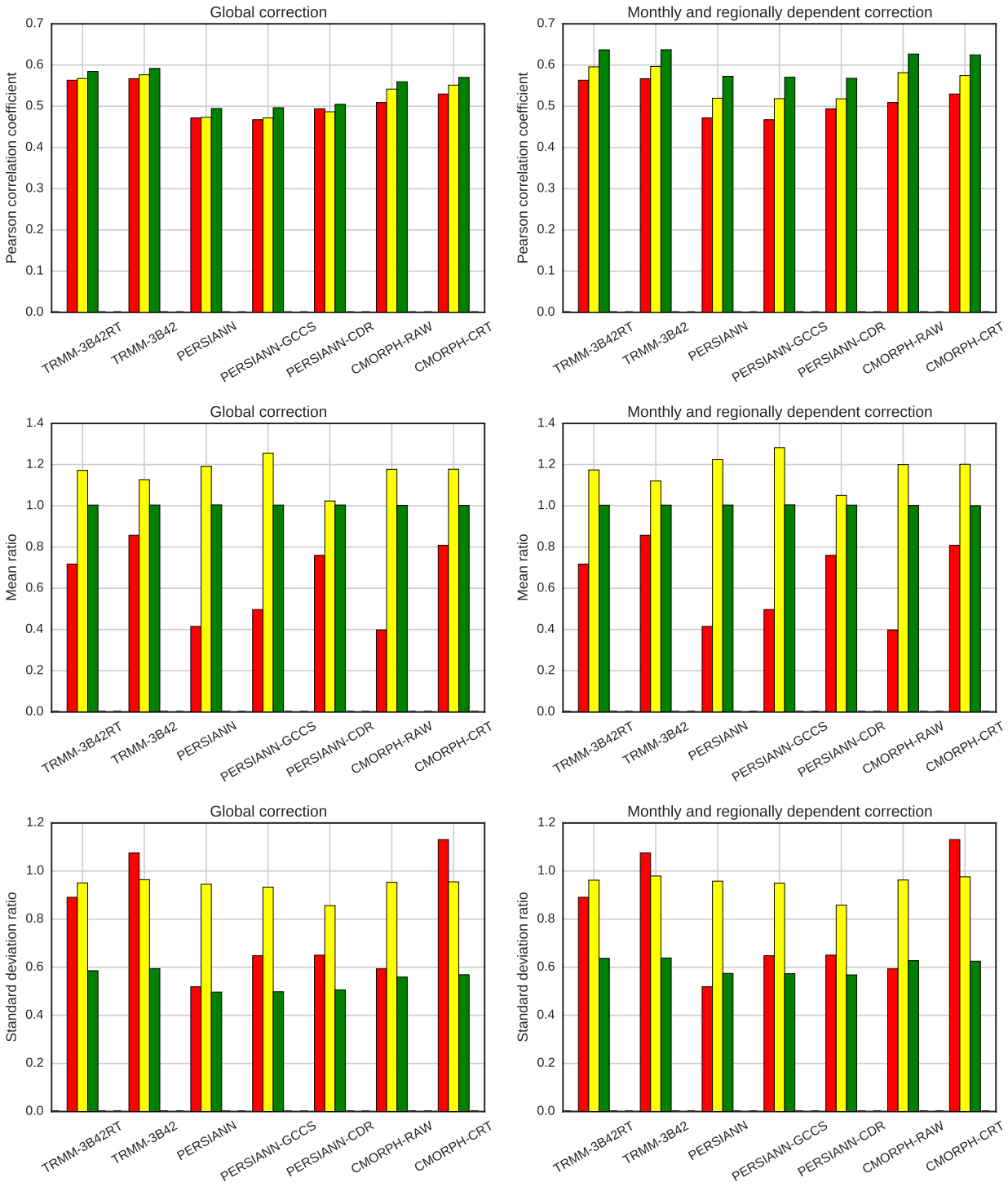
Global correction
Monthly and regionally dependent correction
Pearson correlation coefficient
Mean ratio
Standard deviation ratio
TRMM-3B42RT
TRMM-3B42
PERSIANN
PERSIANN-GCCS
PERSIANN-CDR
CMORPH-RAW
CMORPH-CRT
Raw satellite
Satellite corrected through quantile mapping
Satellite corrected through intensity scaling

FIG. 6. Pearson correlation coefficient (top), mean ratio (middle) and standard deviation ratio (bottom) between the raingage-based and the satellite-based rainfall estimates, without satellite estimate correction (red), using quantile mapping correction (yellow), and using intensity scaling correction (green). Left: global correction. Right: monthly and regionally dependent correction.

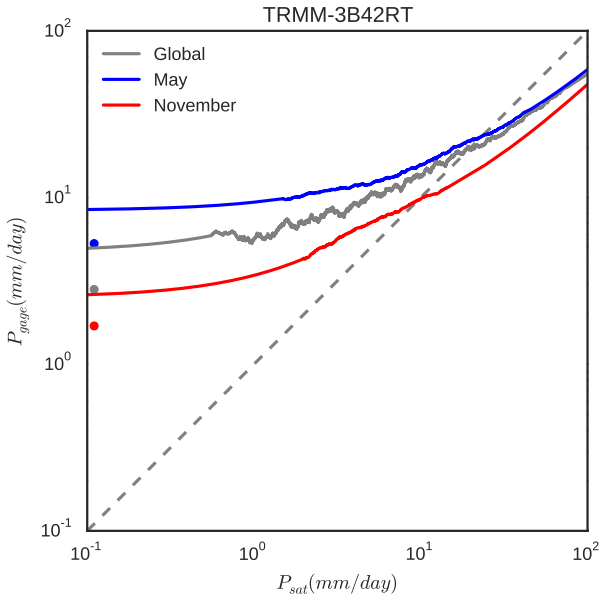

FIG. 7. TRMM-3B42RT monthly dependent correction curve, only shown for the wettest and the driest months, May and November, respectively. The global correction curve (i.e., with no monthly dependence) is represented in gray. The dots represent the corrected satellite values for $P_{sat} = 0$.

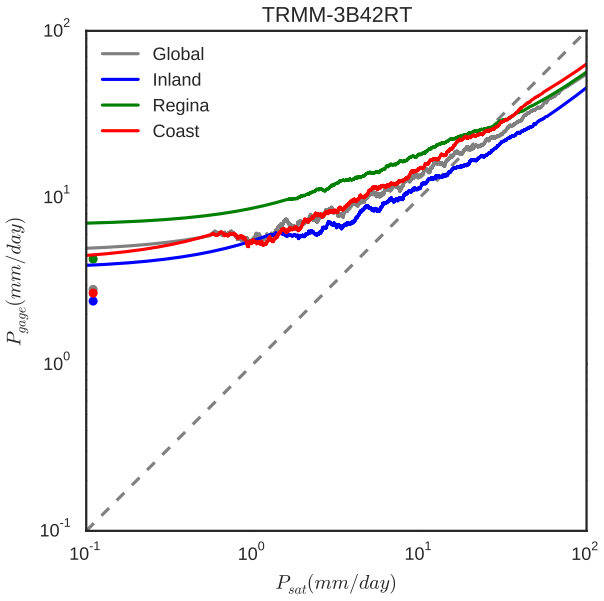

FIG. 9. TRMM-3B42RT regionally dependent correction curve (all months). The global correction curve (i.e., with no monthly or regional dependence) is represented in gray. The dots represent the corrected satellite values for $P_{sat} = 0$.

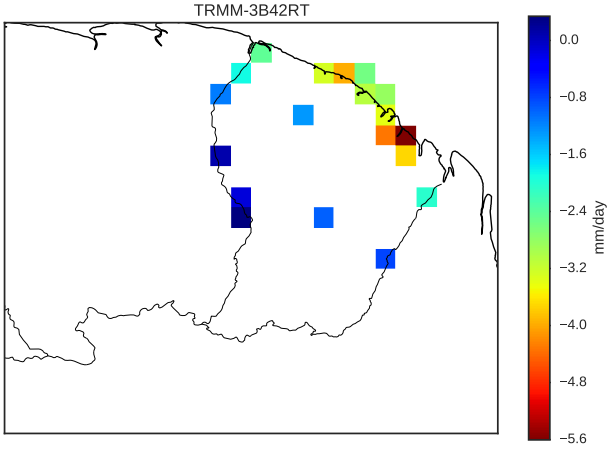

FIG. 8. TRMM-3B42RT total rainfall anomaly for the 2000-03-01 to 2013-12-31 period.

4) MONTHLY AND REGIONALLY DEPENDENT CORRECTION

Since the correction is both monthly and regionally dependent, we combine both dependencies. The point evaluation of the monthly and regionally dependent correction is shown in Figure **??** (right).

Compared to the global correction, there is an increase in the Pearson correlation coefficient for both the quantile mapping and the intensity scaling correction. Compared to the original satellite-based rainfall estimates, the increase in the Pearson correlation coefficient for the intensity scaling correction is about twice the increase for the quantile mapping correction. The mean ratio plot does not show a significant change compared to the global correction, i.e., there is still a positive bias for the quantile mapping correction. For the standard deviation ratio, the results do not change for the quantile mapping correction compared to the global correction, but the intensity scaling correction shows an increase. We conclude that the monthly and regional dependence is justified and that the intensity scaling correction is superior to the quantile mapping correction with regards to the point evaluation.

5) CROSS-VALIDATION

Until now, the correction method was calibrated and tested on the same time period: the period where both

the satellite-based rainfall estimates and the raingage measurements were available (calibration mode). We now wish to assess the performances of the correction method when it is applied outside the calibration period, thus guaranteeing an independent validation and giving results that are more representative of real-world applications (e.g., real time correction, correction on a period where no ground reference was available). The cross-validation technique is used for this purpose. It consists of splitting the time period for which the data set is available in two equal parts, using the first half as a training data set (calibration) and the second half as a testing data set (validation), and then using the second half for the calibration and the first half for the validation.

Figure **??** shows the results of the cross-validation for the quantile mapping and the intensity scaling correction techniques (using monthly and regionally dependent corrections). For the purpose of clarity, we only show the mean of the results over the two subperiods. Overall, the results are very similar to those presented in the right plots of Figure **??**, which are represented as circles in Figure **??** (calibration mode). In cross-validation, there is a small penalty for the Pearson correlation coefficient, both for the quantile mapping and the intensity scaling corrections. The mean ratio and the standard deviation ratio follow the same trend as those presented in calibration mode.

b. Areal (hydrological) evaluation

1) CALIBRATION MODE

Here the hydrological evaluation of the proposed approach is performed in calibration mode, i.e., the four parameters of the GR4J model are calibrated on the whole time period where the rainfall and the discharge are available. Because the various rainfall satellite products do not span the same time period, we reduced the calibration period to the 2000-01-01 to 2012-02-12 period to provide a fair comparison. This calibration period is reduced further for satellite products available after 2000-01-01. In the calibration period, 1 year is used to initialize the hydrological model, and this year is not used for the streamflow validation.

Figure **??** shows the NSE results. When the hydrological model is calibrated with the raingage-based rainfall estimates, the NSE results range from about 0.6 to 0.85. The areal rainfall is derived from the raingage-based rainfall estimates using the Thiessen polygon method. Figure **??** shows that the areal rainfall will not be represented equally well over all the catchments. For instance, only one raingage is located inside the Lawa River catchment at Maripasoula, which is quite large (28,285 km^2). The Maroni River catchment at Langa Tabiki is three times larger (60,930 km^2) and has only four raingages. On the other hand, the Comté River catchment at Saut Bief

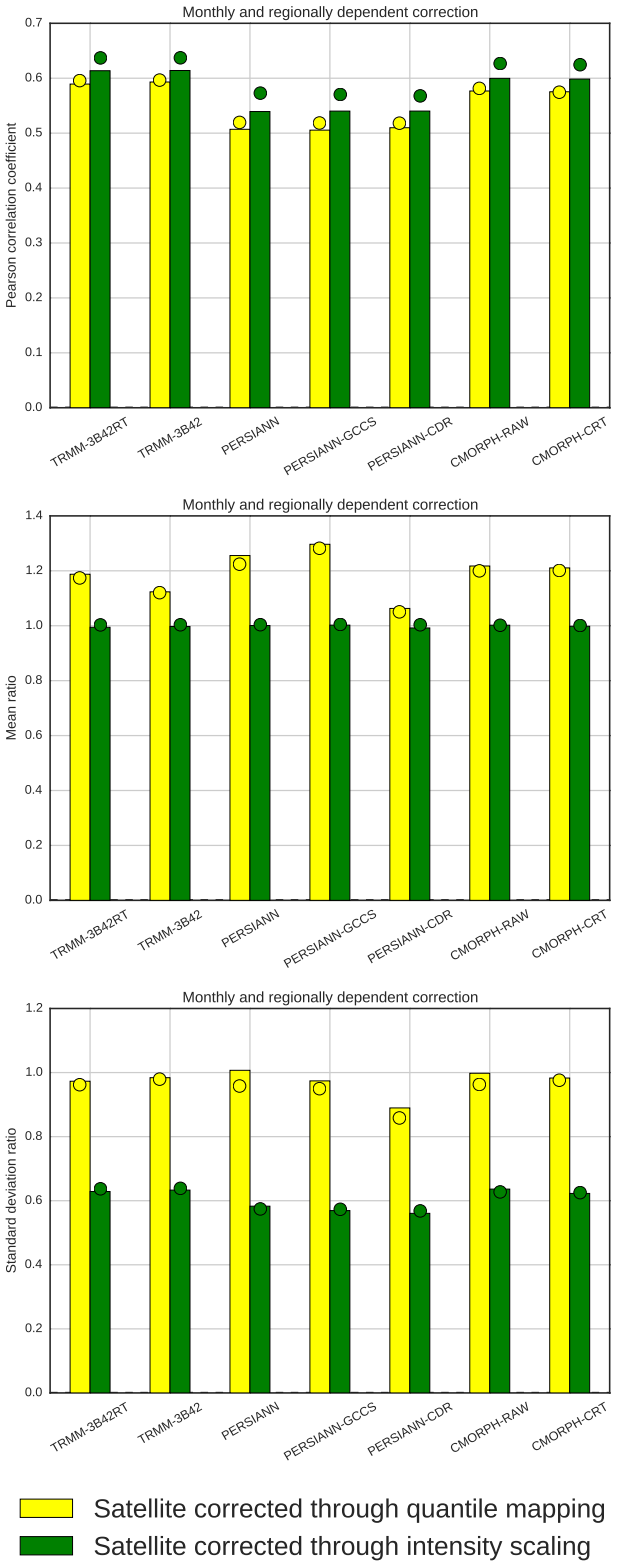

FIG. 10. Cross-validation of the quantile mapping (yellow) and the intensity scaling (green) corrections. Each bar corresponds to the mean of the cross-validation results on both subperiods. The circles show the calibration results.

is quite small (1,760 km^2) and has one raingage. Furthermore, some catchments will be more constrained than others during the calibration (and thus their NSE should be lower), because not all observed streamflow time series are complete (see section **??**). For instance, the observed streamflow time series of the Comté River at Saut Bief is almost complete, while for the Oyapock River at Saut Maripa and for the Mana River at Saut Sabbat only about half the observed streamflow time series is available. These considerations are in accordance with the NSE results. Overall, when the hydrological model is calibrated with the raingage-based rainfall estimates, the NSE results are reasonably good except for the Lawa River catchment at Maripasoula and the Maroni River catchment at Langa Tabiki. The NSE resuts for the original satellite-based rainfall estimates are generally lower than for the raingage-based rainfall estimates. With the quantile mapping correction, the NSE results are always better than the original satellite-based rainfall estimates, but they seem to outperform the raingage-based rainfall estimates only for the Lawa River catchment at Maripasoula and the Maroni River catchment at Langa Tabiki, where the raingage density is very low. With the intensity scaling correction, the NSE results are almost always better than the satellite-based rainfall estimates corrected with the quantile mapping correction.

It is interesting to note that the satellite rainfall products that are bias-corrected (TRMM-3B42 and CMORPH-CRT) do not give better NSE results than their real time versions (i.e., those not bias-corrected) for the Lawa River catchment at Maripasoula and the Maroni River catchment at Langa Tabiki, probably because of their relatively low raingage density. After intensity scaling correction, the difference in NSE efficiency between real time and bias-corrected satellite products is generally no longer visible. This means that using the intensity scaling correction, there is no reason to favor a bias-corrected satellite rainfall product over its real time version. This is an important result because real time satellite-based rainfall estimates can now be used for hydrological forecasting with the same level of confidence as their bias-corrected versions (which are not real time estimates), using the intensity scaling correction method.

2) CROSS-VALIDATION

Here we use the correction methods that make use of the whole time period where the raingage measurements are available for their calibration (calibration mode), attempting to hydrologically assess the performance of the corrected rainfall in cross-validation. Therefore, the 2000-01-01 to 2012-02-12 period is split into two equal parts, first calibrating the GR4J model on the first half and validating it on the second half, then calibrating it on the second half and validating it on the first half. The results are shown in Figure **??**.

Because the number of missing data in the streamflow time series greatly varies from one catchment to another, the results should be interpreted with care. The NSE results between the two subperiods can be very different because there is not necessarily the same number of streamflow data in the two subperiods. For the purpose of clarity, we only show the mean of the NSE results over the two subperiods. Overall, the NSE results in cross-validation follow the same trend as the NSE results in calibration mode, and the superiority of the intensity scaling correction over the quantile mapping correction remains true. In conclusion, the intensity scaling correction method performs better than the quantile mapping correction method when it is tested hydrologically on a time period that is independent of the time period on which the hydrological model was calibrated.

5. Discussion

It can be argued that one of the drawbacks of the intensity scaling method is that there can no longer be a zero rainfall estimate after applying the correction. This is indeed a limitation of this method, although the quantile mapping method also suffers from this limitation. **?** addressed this problem by modeling the rainfall occurence rate and randomly generating zero rainfall intensities, thus guaranteeing that the generated rainfall occurence rate is in accordance with the observed rainfall. It should be noted however, that no extra information is created using this method, essentially because it is based on a stochastic (i.e., random) generation. One simulation run of the model could generate the correct occurrence of rainfall, and next an incorrect one. Since the rainfall occurence is not captured by the satellites, this information is permanently lost. In this study, we prefer having deterministic (i.e., reproductible) results. Furthermore, from a hydrological point of view, the importance of having zero rainfall intensities is relative, because of the smoothing effect of the catchment and the attenuation effect of evapotranspiration. Rather than the strict occurrence of rainfall, a better estimation of rainfall variability is more important.

Figure **??** shows the mean annual satellite-based rainfall estimates over French Guiana from 2003-01-01 to 2012-12-31 (10 years), for TRMM-3B42RT, PERSIANN and CMORPH-RAW. Even though the three satellite rainfall products show very different mean estimates before correction (left), they are much more similar after correction (right). The convergence of these results gives further confidence in the intensity scaling correction.

6. Conclusion

This paper has presented an intensiy scaling technique for correcting satellite-based rainfall estimates, which

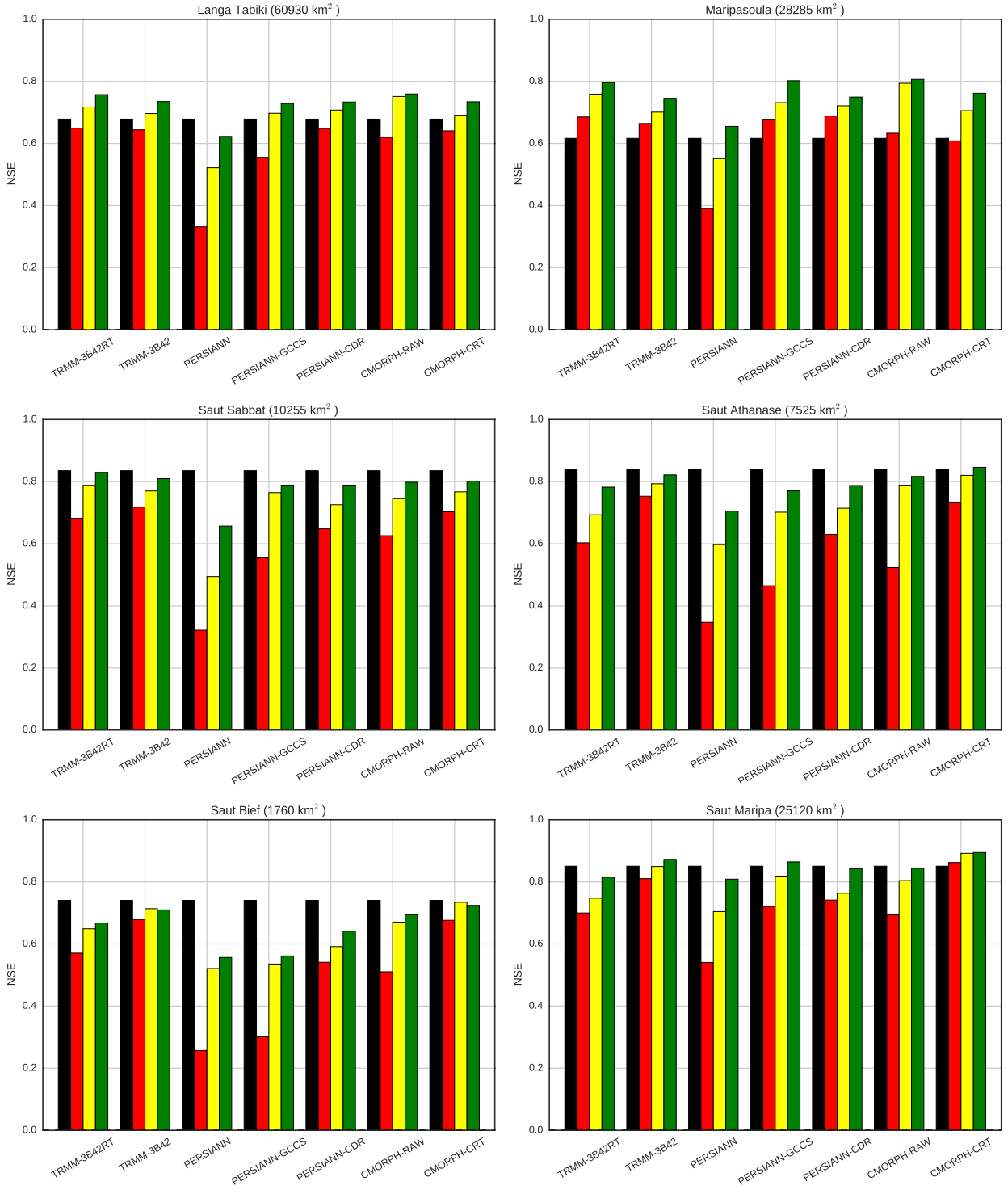
Langa Tabiki (60930 km^2)
Maripasoula (28285 km^2)
Saut Sabbat (10255 km^2)
Saut Athanase (7525 km^2)
Saut Bief (1760 km^2)
Saut Maripa (25120 km^2)
NSE
0.0
0.2
0.4
0.6
0.8
1.0
TRMM-3B42RT
TRMM-3B42
PERSIANN
PERSIANN-GCCS
PERSIANN-CDR
CMORPH-RAW
CMORPH-CRT
Raingage
Raw satellite
Satellite corrected through quantile mapping
Satellite corrected through intensity scaling

FIG. 11. Nash-Sutcliffe model efficiency between the simulated and the observed streamflows for the six gauged catchments in French Guiana, with raingage-based rainfall estimates (black), original satellite-based rainfall estimates (red), using quantile mapping (yellow) and intensity scaling correction (green). The correction is monthly and regionally dependent.

consists of taking the mean of the raingage-based rainfall estimates given the satellite-based rainfall estimates (conditional mean). This correction method shows better results than the quantile mapping technique, which is usually used for this purpose. The intensity scaling correction method has been refined both in time, through a monthly calibration, and in space, through a regional calibration. The hydrological validation shows results that suggest the possibility of using the corrected rainfall estimates for operational hydrological forecasting purposes. In French Guiana, as in many countries of the world where the raingage network is insufficient for a direct hydrological use (or simply not available in real time) but sufficient to calibrate this simple correction method, the use of satellite-based rainfall estimates could become a valuable option for real time applications.

As a perspective, one could use the conditional distribution of the ground truth given the satellite-based rainfall estimates (instead of the conditional mean) to generate possible rainfall scenarios. This would allow to propagate the satellite-based rainfall estimate uncertainty through a hydrological model, thus providing a probabilistic information on the simulated streamflow, which can be of crucial importance for hydrological applications (**?**).

Acknowledgments. This work was supported by a grant from *SCHAPI* and *ONEMA*. The authors would like to thank *Météo France* and *DEAL Guyane* for providing rainfall gage measurements and streamflow measurements, respectively. Also, Prof. Soroosh Sorooshian and the PERSIANN team at UC Irvine for their kind assistance.

References

Andréassian, V., C. Perrin, C. Michel, I. Usart-Sanchez, and J. Lavabre, 2001: Impact of imperfect rainfall knowledge on the efficiency and the parameters of watershed models. *Journal of Hydrology*, **250 (14)**, 206 – 223.

Beucher, F., 2010: *Météorologie tropicale : des alizés au cyclone*. Cours et manuels - Direction de la météorologie, La Documentation Française.

Gebremichael, M., and F. Hossain, 2009: *Satellite Rainfall Applications for Surface Hydrology*. Springer.

Gosset, M., J. Viarre, G. Quantin, and M. Alcoba, 2013: Evaluation of several rainfall products used for hydrological applications over West Africa using two high-resolution gauge networks. *Quarterly Journal of the Royal Meteorological Society*, **139 (673)**, 923–940.

Gudmundsson, L., J. B. Bremnes, J. E. Haugen, and T. Engen-Skaugen, 2012: Technical note: Downscaling RCM precipitation to the station scale using statistical transformations - a comparison of methods. *Hydrology and Earth System Sciences*, **16 (9)**, 3383–3390, doi:10.5194/hess-16-3383-2012, URL http://www.hydrol-earth-syst-sci.net/16/3383/2012/.

Hirpa, F. A., M. Gebremichael, and T. Hopson, 2010: Evaluation of high-resolution satellite precipitation products over very complex terrain in ethiopia. *Journal of Applied Meteorology and Climatology*, **49 (5)**, 1044–1051, doi:10.1175/2009JAMC2298.1, URL http://journals.ametsoc.org/doi/abs/10.1175/2009JAMC2298.1.

Hsu, K., X. Gao, S. Sorooshian, and H. Gupta, 1997: Precipitation estimation from remotely sensed information using artificial neural networks. *Journal of Applied Meteorology*, **36 (9)**, 1176–1190.

Hu, Q., D. Yang, Y. Wang, and H. Yang, 2013: Accuracy and spatiotemporal variation of high resolution satellite rainfall estimate over the Ganjiang River Basin. *Science China Technological Sciences*, **56 (4)**, 853–865.

Huffman, G. J., and Coauthors, 2007: The TRMM multisatellite precipitation analysis (TMPA): Quasi-global, multiyear, combined-sensor precipitation estimates at fine scales. *Journal of Hydrometeorology*, **8 (1)**, 38–55.

Joyce, R., J. Janowiak, P. Arkin, and P. Xie, 2004: CMORPH: A method that produces global precipitation estimates from passive microwave and infrared data at high spatial and temporal resolution. *Journal of Hydrometeorology*, **5 (3)**, 487–503.

Maggioni, V., H. J. Vergara, E. N. Anagnostou, J. J. Gourley, Y. Hong, and D. Stampoulis, 2013: Investigating the Applicability of Error Correction Ensembles of Satellite Rainfall Products in River Flow Simulations. *Journal of Hydrometeorology*, **14 (4)**, 1194–1211, doi:10.1175/JHM-D-12-074.1, URL http://journals.ametsoc.org/doi/abs/10.1175/JHM-D-12-074.1.

Müller, M. F., and S. E. Thompson, 2013: Bias adjustment of satellite rainfall data through stochastic modeling: Methods development and application to Nepal. *Advances in Water Resources*, **60**, 121–134, doi:10.1016/j.advwatres.2013.08.004, URL http://linkinghub.elsevier.com/retrieve/pii/S0309170813001358.

Nash, J., and J. Sutcliffe, 1970: River flow forecasting through conceptual models part I – A discussion of principles. *Journal of Hydrology*, **10 (3)**, 282 – 290.

Nelder, J. A., and R. Mead, 1965: A simplex method for function minimization. *The computer journal*, **7 (4)**, 308–313, URL http://comjnl.oxfordjournals.org/content/7/4/308.short.

Oudin, L., C. Michel, and F. Anctil, 2005: Which potential evapotranspiration input for a lumped rainfall-runoff model? *Journal of Hydrology*, **303 (1-4)**, 275–289, doi:10.1016/j.jhydrol.2004.08.025, URL http://linkinghub.elsevier.com/retrieve/pii/S0022169404004044.

Perrin, C., C. Michel, and V. Andréassian, 2003: Improvement of a parsimonious model for streamflow simulation. *Journal of Hydrology*, **279 (1-4)**, 275–289.

Roche, M. A., 1982: Evapotranspiration réelle de la forêt amazonienne en Guyane. *Cahier Orstom. Série: Hydrologie*, **19 (1)**, 37–44.

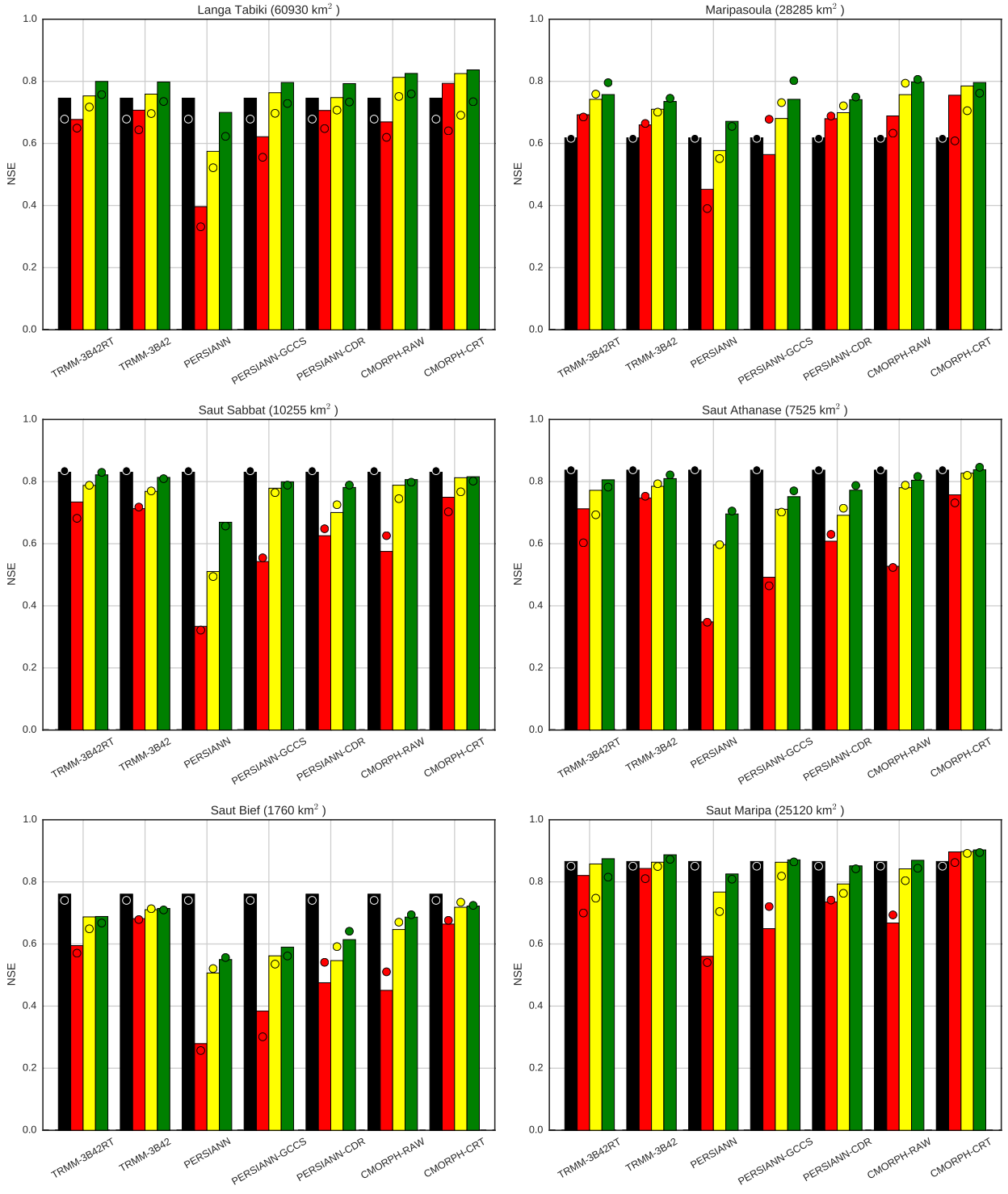
Langa Tabiki (60930 km^2)
Maripasoula (28285 km^2)
Saut Sabbat (10255 km^2)
Saut Athanase (7525 km^2)
Saut Bief (1760 km^2)
Saut Maripa (25120 km^2)
NSE
0.0
0.2
0.4
0.6
0.8
1.0
TRMM-3B42RT
TRMM-3B42
PERSIANN
PERSIANN-GCCS
PERSIANN-CDR
CMORPH-RAW
CMORPH-CRT
Raingage
Raw satellite
Satellite corrected through quantile mapping
Satellite corrected through intensity scaling

FIG. 12. Cross-validation of the hydrological model when using raingage-based rainfall estimates (black), original satellite-based rainfall estimates (red), quantile mapping corrected satellite rainfall (yellow) and intensity scaling corrected satellite rainfall (green). Each bar corresponds to the mean of the cross-validation results on both subperiods. The circles show the calibration results.

Sapiano, M. R. P., and P. A. Arkin, 2009: An intercomparison and validation of high-resolution satellite precipitation estimates with 3-hourly gauge data. *Journal of Hydrometeorology*, **10 (1)**, 149–166, doi:10.1175/2008JHM1052.1, URL http://journals.ametsoc.org/doi/abs/10.1175/2008JHM1052.1.

Serrat-Capdevila, A., J. B. Valdes, and E. Z. Stakhiv, 2014: Water management applications for satellite precipitation products: Synthesis and recommendations. *JAWRA Journal of the American Water Resources Association*, **50 (2)**, 509–525.

Tian, Y., C. D. Peters-Lidard, and J. B. Eylander, 2010: Real-Time Bias Reduction for Satellite-Based Precipitation Estimates. *Journal of Hydrometeorology*, **11 (6)**, 1275–1285, doi:10.1175/2010JHM1246.1, URL http://journals.ametsoc.org/doi/abs/10.1175/2010JHM1246.1.

Tobin, K. J., and M. E. Bennett, 2010: Adjusting Satellite Precipitation Data to Facilitate Hydrologic Modeling. *Journal of Hydrometeorology*, **11 (4)**, 966–978, doi:10.1175/2010JHM1206.1, URL http://journals.ametsoc.org/doi/abs/10.1175/2010JHM1206.1.

Zulkafli, Z., W. Buytaert, C. Onof, B. Manz, E. Tarnavsky, W. Lavado, and J.-L. Guyot, 2014: A Comparative Performance Analysis of TRMM 3B42 (TMPA) Versions 6 and 7 for Hydrological Applications over AndeanAmazon River Basins. *Journal of Hydrometeorology*, **15 (2)**, 581–592, doi:10.1175/JHM-D-13-094.1, URL http://journals.ametsoc.org/doi/abs/10.1175/JHM-D-13-094.1.

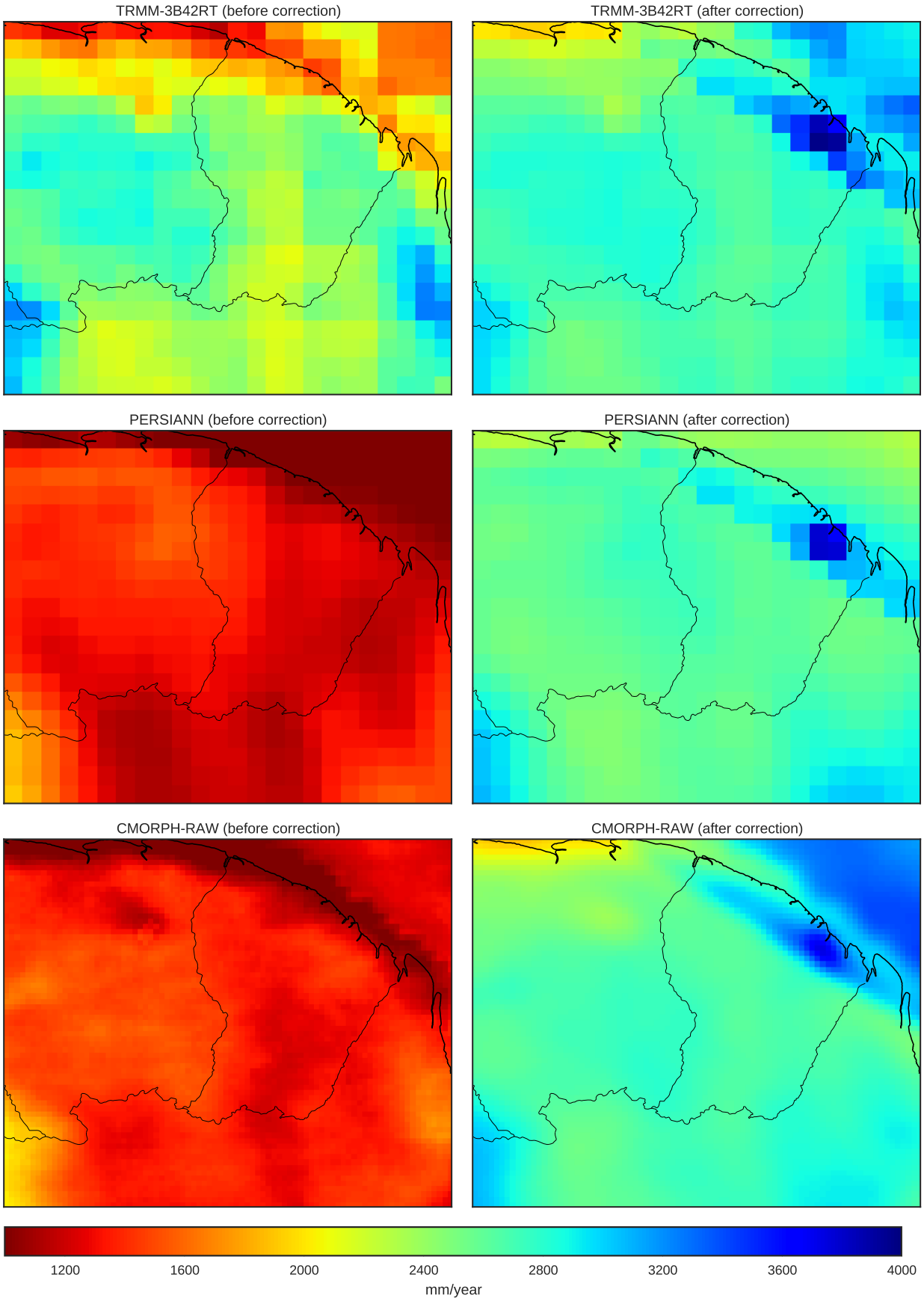
TRMM-3B42RT (before correction)
TRMM-3B42RT (after correction)
PERSIANN (before correction)
PERSIANN (after correction)
CMORPH-RAW (before correction)
CMORPH-RAW (after correction)
1200
1600
2000
2400
2800
3200
3600
4000
mm/year

FIG. 13. Mean annual satellite-based rainfall estimates over French Guiana from 2003-01-01 to 2012-12-31. Left: before correction. Right: after monthly and regionally dependent intensity scaling correction.